Physics of Fluids

RESEARCH ARTICLE | MARCH 30 2021

Prediction of droplet sizes in a T-junction microchannel: Effect of dispersed phase inertial forces

Santosh Kumar Jena ; Supreet Singh Bahga ; Sasidhar Kondaraju

Physics of Fluids 33, 032120 (2021)
https://doi.org/10.1063/5.0039913

Physics of Fluids ARTICLE scitation.org/journal/phf

Prediction of droplet sizes in a T-junction microchannel: Effect of dispersed phase inertial forces

Cite as: Phys. Fluids **33**, 032120 (2021); doi: 10.1063/5.0039913
Submitted: 8 December 2020 · Accepted: 24 February 2021 ·
Published Online: 30 March 2021

Santosh Kumar Jena,[1] Supreet Singh Bahga,[2] and Sasidhar Kondaraju[1,a)]

AFFILIATIONS

[1]School of Mechanical Sciences, Indian Institute of Technology Bhubaneswar, Argul, Khurda 752050, Odisha, India
[2]Department of Mechanical Engineering, Indian Institute of Technology Delhi, Hauz Khas 110016, New Delhi, India

[a)]**Author to whom correspondence should be addressed:** sasidhar@iitbbs.ac.in. **URL:** https://www.iitbbs.ac.in/profile.php/sasidhar

ABSTRACT

The generation of monodispersed droplets in T-junction microchannels has wide range applications in biochemical analysis and material synthesis. While the generation of these monodispersed droplets was previously considered to be a balance between forces acting from continuous phase and interfacial force, it is shown here that the inertial force from the dispersed phase also plays an important role in determining the size of the generated droplets. A theoretical analysis for the size of monodisperse droplets generated in a microfluidic T-junction device is developed, and it is validated with a large set of experimental observations. The theoretical analysis accounts for the inertial forces from the dispersed phase along with the forces from the continuous phase and the interfacial forces to define the non-dimensional numbers that govern the droplet breakup in the T-junction microchannel.

I. INTRODUCTION

Due to the immiscible nature of two fluids and scaling benefits, droplet microfluidics attracts many researchers to a great extent. The various droplet operations like droplet generation, droplet fission, droplet fusion, mixing, and droplet sorting along with their application are thoroughly described by Teh *et al.*[1] Baroud and co-workers[2] widely studied the different geometry for performing different droplet operations and how the flow field is affected in the presence of droplets during transport inside the microchannel. Besides, the effect of geometry, wettability on droplet generation along with certain fabrication techniques and in-depth understanding of droplet microfluidics are widely investigated by several authors.[3,4] Among various categories of droplet microfluidics, droplet generation inside a microchannel is one of the most vital phases.[5–7] The formation of the droplet in squeezing regime inside flow focusing (cross junction) channel was studied by Loo *et al.*[8] without and with the addition of surfactant to continuous phase and through empirical relation reveals that the droplet volume is a function of both the Capillary number (Ca) and flow rate ratio (ϕ). Moreover, recently, Wu *et al.*[9] investigated the formation of droplet and found four regimes like slug, dripping, jetting, and viscous displacement. They show that the droplet size is controlled by the flow rate of both the continuous and dispersed phases and the capillary number of the continuous phase (Ca_c) and dispersed phase (Ca_d) firmly affects the four regimes. The pressure profile of the dispersed phase and continuous phase during the breakup of droplet generation and the effect of viscosity ratio, flow rate ratio, and Ca_c on pressure jump across the droplet in the T-junction were explored in detail.[10,11] As discrete volumes of droplets are created using droplet microfluidics, many reactions are possible without increasing the device size and complexity.[12] Due to its wide range of applications in biology,[13–15] drug delivery,[4,7] medical diagnostics,[16] and nanodevice fabrications,[4,14] precise control of monodispersed droplets is very much a pivotal issue. Among active[17,18] and passive droplet generation methods,[19,20] passive methods are widely used due to the ease of fabrication, where the deformation and breakup of interface occur due to geometry and flow rate. Due to the simple fabrication technique and allowing for synchronized monodispersed droplet production, T-junction is a widely used passive technique in the droplet-based microfluidics.

Formation of droplets using T-junction microchannels was first proposed by Thorsen *et al.*[21] They predicted that the size of the droplet generated in a T-junction microchannel depends on the relative magnitude of shear forces and interfacial forces. Later, Nisisako *et al.*[22] performed experiments by varying the continuous phase and the dispersed phase flow rates and observed that the droplet size and its

production rate could be controlled by varying both the flow rates independently. Stone and co-workers[23] showed that at very low capillary numbers where interfacial forces dominate the shear forces, the breakup of droplet occurs due to the high resistance to the flow of the continuous phase, which leads to high pressure difference at the front and rear ends of the dispersed phase. Using a scaling analysis, they showed that the non-dimensional length of the droplets depends on the ratio of the dispersed phase and the continuous phase flow rates. The same group had later suggested that the droplet generation in T-junction microchannels follows three different regimes, i.e., squeezing, dripping, and jetting, where the squeezing and dripping regimes are stable regimes, and the jetting is mostly an unstable regime.[24] The non-dimensional numbers, which were considered important for controlling the droplet generation in microfluidics, are the capillary number of the continuous phase, $Ca_c = \mu_c U_c/\sigma$, flow rate ratio, $\phi = Q_d/Q_c$, and viscosity ratio, $\lambda = \mu_d/\mu_c$,[24–31] where μ_c is the viscosity of the continuous phase, Q is the flow rate, U_c is the average velocity of the continuous phase, and σ is the interfacial tension. The subscripts c and d represent the continuous phase and dispersed phase, respectively. Various correlations and scaling laws for different droplet generation regimes were proposed in the past two decades using the non-dimensional parameters.[23,26,32–34] In the squeezing regime, the models proposed to estimate the droplet generation in T-junction microchannels are dependent on the experimental fitting parameters and do not work universally. No scaling laws have been proposed to predict the droplet sizes in the dripping and the jetting regimes. The force balance models, which were used for droplet generation, do not accurately predict the experimental results reported. To date, there exists no generalized model that can predict the size of the droplet in all stable regimes of droplet formation in a T-junction microchannel. It is also important to note that the dispersed phase Weber number, $We_d = \rho_d U_d^2 w_d/\sigma$, is also considered to govern the droplet generation in co-flow microfluidic,[35] but no attempt has been made to study the effect of the dispersed phase inertial forces on droplet generation in a T-junction microchannel.

In the present study, a model is developed, by formulating the external forces using scaling principles, to estimate the length of the droplets generated in a T-junction microchannel. It is shown that the inertial forces from the dispersed phase play an important role in governing the breakup of the droplet in a T-junction microchannel. It is also shown that there exists a common power law to account for droplet sizes in both squeezing and dripping regimes. The proposed model accounts for the inertial forces of the dispersed phase along with the forces due to the continuous phase and the interfacial force. The model formulated in the present study is compared with experiments performed by the authors as well as those from the existing literature. The results show that the data for a set of continuous and dispersed phase fluids collapses into a single curve for varying flow rate ratios.

II. MATHEMATICAL FORMULATION

In a typical process of droplet formation in a T-junction microchannel device, the continuous phase fluid flows in the main channel, and the dispersed phase fluid is pumped through an orthogonal channel, as shown in Fig. 1. The dispersed phase fluid penetrates the main channel and an interface between the continuous and dispersed phase fluids is formed. The interface deforms downstream due to the flow from the main channel and forms a neck shape, as shown in Fig. 1.

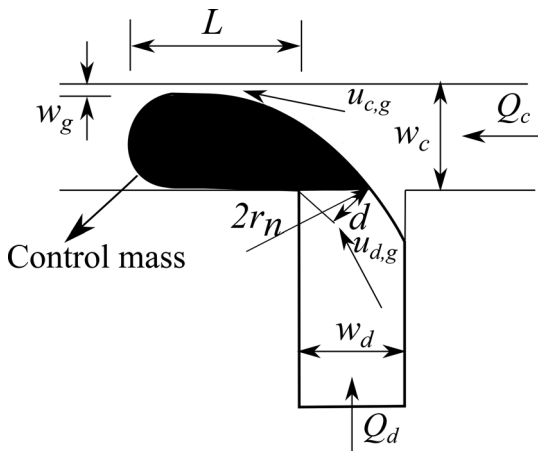

FIG. 1. A schematic representation of the shape of interface (in top view).

Further deformation of the interface due to either pressure differences or the shear forces from the continuous phase creates a kink in the neck, leading to pinch off of droplet from the dispersed phase fluid. Important length parameters that affect the droplet formation are shown in the figure. The widths of the main and orthogonal channels are w_c and w_d, respectively. The distance between the wall and the interface, and the length of the interface from the tip to the corner of the T-junction before the kink formation on the interface are given as w_g and L, respectively. The radius of curvature of the neck is $2r_n$, and d is the neck thickness measured at an angle of 45° from the corner of the junction. The velocity of the continuous phase fluid in w_g is given as $u_{c,g}$ and the dispersed phase fluid velocity at the neck region is given as $u_{d,g}$. The shaded portion shown in Fig. 1 is considered as the control mass.

Forces acting on the control mass account for the rate of change of its momentum as described by Newton's second law of motion. At critical size when droplet breaks up, we can write $d(mu)/dt = \sum F_{external}$,

$$F_\tau + F_p - F_\sigma = \frac{d(mu)}{dt}, \tag{1}$$

where m is the mass of the control mass and u is the velocity of the control mass. External forces acting on the control mass are the force due to pressure difference at the leading and trailing interfaces of the droplet (F_p), the shear forces from the continuous phase (F_τ), and the interfacial force (F_σ). The pressure and shear forces act in a way to detach the control mass from the dispersed phase fluid, and the interfacial force acts to resist the deformation of control mass. If $w_g \ll w_c$, we can estimate the forces due to pressure difference using lubrication analysis as $F_p = \Delta p w_c h \sim O(\mu Q_c w_c L/w_g^3)$. Here, h is the depth of the channel. The shear forces acting on the control mass can be considered as $F_\tau = \tau w_c h \sim O(\mu Q_c L/w_g^2)$, and the interfacial force can be estimated as $F_\sigma \sim \sigma h$. For a detailed derivation of forces acting on the control mass, the readers are referred to Garstecki *et al.*[23] In the squeezing regime (where $w_g \ll w_c$), $F_p \gg F_\tau$ and in the dripping regime F_τ dominates over F_p. Using the external forces, the equation [Eq. (1)] governing the motion of control mass can be written as

$$\mu_c U_c l_d \left(\frac{w_c}{w_g}\right)^2 h + \mu_c U_c l_d \left(\frac{w_c}{w_g}\right)^3 h - \sigma h \sim m\frac{du}{dt} + u\frac{dm}{dt}. \quad (2)$$

The ratio of the length of the droplet with the width of the continuous phase channel is the non-dimensional length of the droplet, $l_d = L/w_c$. The control mass moves with almost a constant velocity, and hence we can consider that the rate of velocity change of the control mass is zero. The rate of change of control mass is constant, controlled by the dispersed phase flow rate, Q_d. Hence, $dm/dt = \rho_d U_d w_d h$. The forces presented here will be applicable for the microchannels where the channel depths are of the same order of magnitude as the width of the channel. However, when the channel depth is reduced such that the flow is shallow, large velocity gradients over the channel depth can change the magnitude of shear forces acting on the droplet. Hence, the proposed model cannot be applied for predicting the droplet sizes for channels with narrow depths. Equation (2) can be rearranged as follows:

$$\mu_c U_c l_d \left(\frac{w_c}{w_g}\right)^2 h + \mu_c U_c l_d \left(\frac{w_c}{w_g}\right)^3 h \sim \sigma h + \rho_d U_d w_d h u,$$

i.e.,

$$\mu_c U_c l_d h \left[\left(\frac{w_c}{w_g}\right)^2 + \left(\frac{w_c}{w_g}\right)^3\right] \sim \sigma h + \rho_d U_d w_d h u. \quad (3)$$

From Eq. (3), we can see that the inertial forces from the dispersed phase also govern the size of the droplet generated in a T-junction microchannel. The physical explanation for the effect of dispersed phase inertial forces can be thought of as the resistance developed by the dispersed phase to the squeezing of the neck in terms of dynamic pressure. In the current model, the inertia of the continuous phase is not taken into consideration as the inertial force of the continuous phase will lead to an unstable increase in the dispersed phase thread, which is termed as a jetting regime. The jetting regime is not useful since the thread length cannot be controlled and hence the droplet generation will fail eventually. However, if the dispersed phase flow rates are high, irrespective of the continuous phase velocities, the dispersed phase elongates further down the channel and the droplet breakup will occur due to jetting instability instead of the shear along the neck region. Our experimental evidence concludes that the formation of droplets got affected by the dispersed phase inertia force rather than inertia of continuous phase. The jetting regime was recently observed by Korczyk *et al.*,[36] where they found that the droplet generation transforms directly from squeezing regime to jetting regime without the thinning of the neck. The velocity u of the control mass will depend on the U_c or U_d depending on whichever is larger. Here, u is scaled as an average of U_c and U_d, i.e., $u \sim (U_c + U_d)/2$. Since $U_d/U_c = w_c\phi/w_d$, $u \sim U_d(w_d/w_c + \phi)/2\phi$. In the present study, the widths of the dispersed phase and continuous phase channels were the same in all the experiments, and hence, u reduces to $u \sim U_d(1+\phi)/2\phi$. It should be noted that in the squeezing regime, the second term on LHS dominates over the first term and vice versa in the dripping regime. Both dripping and squeezing regimes depend on the non-dimensional w_c/w_g, which is not known. By rewriting the terms related to w_c/w_g as a $f(w_c/w_g)$, Eq. (3) is rewritten as

$$l_d Ca_c f\left(\frac{w_c}{w_g}\right) \sim 1 + We_d \frac{1+\phi}{2\phi}. \quad (4)$$

III. MATERIALS AND METHODS

To verify the above model, a large set of experiments were performed by using silicone oil, mineral oil, and hexadecane oil as continuous phase fluids (Sigma Aldrich) while keeping distilled water (DIW) as the dispersed phase. The continuous phase fluids were chosen to obtain large viscosity ratio contrasts. The physical properties of the fluids and flow parameters varied in experiments are given in Table I. The viscosity was measured using a rheometer and Oswald viscometer. The rheometer used for measuring viscosity was the Cone and Plate type measuring system (Anton Paar, CP25-2). The cone diameter is 24.976 mm, and the cone angle is 1.993°. The Oswald viscometer used was a U-tube type glass viscometer. The viscosity curves for mineral oil and silicone oil are shown in Fig. S1. The interfacial tension was measured using the pendant drop method[37] by using the Apex instrument droplet dispenser. First, the surface tension of distilled water (DIW) with respect to air was measured with an accuracy of 98%. For measuring the interfacial tension of oil with respect to DIW, a water droplet is injected into the oil contained in a rectangular beaker and the images are taken by a high-speed camera (Photron FASTCAM mini UX). After that, the image processing was carried out using ImageJ software and interfacial tension was calculated. For fabrication of microchannel, Computer Numerical Control (CNC) micromilling (The Cool Tool®) and thermal bonding techniques were employed. The parameters employed for fabricating the channel in CNC micromilling are spindle speed (rpm), feed rate (mm/min), and depth of cut (μm). After performing the design of experiments (DOE) in Minitab software, we use 50 μm depth of cut, the spindle speed as 3500 rpm, and the feed rate as 25 mm/min for all channel preparations. After that, the microchannel is sealed using another PMMA thin sheet of 5 mm thickness using the thermal bonding technique. The thermal bonding technique is employed using a hot plate, in which a temperature of 170 °C is maintained to seal the two sheets of PMMA. At this temperature, the acrylic (PMMA) sheets were kept for 35–45 min and then allowed to cool for 20–30 min. Finally, the microchannel is prepared and ready for chemical treatment. A T-junction microchannel was fabricated on a polymethyl methacrylate (PMMA) sheet of dimension 50 mm × 30 mm × 5 mm using an end mill of 200 μm diameter. The depth of each channel was 200 μm. The width of the channels in which mineral oil was used as the continuous phase was 300 μm, and the width of the channels in which silicone oil and hexadecane were used as the continuous phase was 280 μm. The total length of the

TABLE I. The range of flow parameters varied in the present experiments, and the physical properties of continuous phase fluids are given here. Distilled water (DIW) is used as a dispersed phase fluid in the present experiments. The properties of DIW are $\mu_d = 0.99$ mPa s and $\rho_d = 1000$ kg/m^3.

Continuous phase	Q_c (μl/min)	ϕ	λ	σ (mN/m)
Hexadecane	29–1234	0.25, 0.5, 1.0	0.4167	44.0
Mineral oil	3–1527	0.25, 0.5, 1.0, 1.5	0.0422	42.3
Silicone oil	7–436	0.25, 0.5, 1.0, 1.5	0.0111	34.8

channel is 30 mm, and the distance from the inlet of the continuous phase to T-junction and the inlet of the dispersed phase to T-junction is 9 mm each. The channels were made hydrophobic by treating with aquapel solution (Pittsburgh Glass Works LLC., USA), and the roughness of the channels measured using an optical profilometer (Wyko NT9100 US) was found to be less than 3 μm. A schematic representation of the experimental setup is shown in Fig. 2. A dual channel syringe pump (Holmarc Inc.) was used for pumping the fluids, and no surfactants were used in either phase. An inverted microscope (Olympus, Japan) was used to visualize droplet formation and capture the phenomena. The droplet formations were captured using a high-speed camera (Photron FASTCAM mini UX) by recording the data at 10 000 fps with a resolution of 1280 × 480 pixels and an exposure time of 100 μs. The data are analyzed using Photron FASATCAM viewer and ImageJ software. All the experiments were carried out at a controlled temperature of 25 °C. Each experiment was conducted three times, and l_d is taken as the average of three experimental runs.

IV. RESULTS AND DISCUSSIONS

Monodispersed droplets of water-in-oil were produced by pumping oil in the continuous phase channel and water in the dispersed phase channel. Three different droplet breakup regimes were observed (i.e., squeezing, dripping, and jetting regimes) during the droplet formations. The squeezing regime is observed at small capillary numbers, and with the increasing capillary number, the droplet breakup transits to the dripping regime and then to the jetting regime, as shown in Fig. 3. The experimental images of the droplet breakup are shown for water droplets in mineral oil. From Fig. 3, it can also be observed that the length of the droplet decreases with an increase in the continuous phase capillary number. The droplet's non-dimensional length measured from experimental results is plotted against the capillary number with varying flow rate ratios and varying viscosity ratios, as shown in Fig. 4. The non-dimensional length l_d of the droplet decreases with an increase in capillary number Ca_c. The droplet breakup follows the squeezing regime at low capillary numbers and transits to the dripping regime and then to the jetting regime. It can be observed from Fig. 4 that the non-dimensional length increases with an increase in flow rates for a given viscosity ratio (λ). In the literature,[38] it was shown that when λ is less than one, there is more reduction of droplet size as compared to a λ greater than one for an

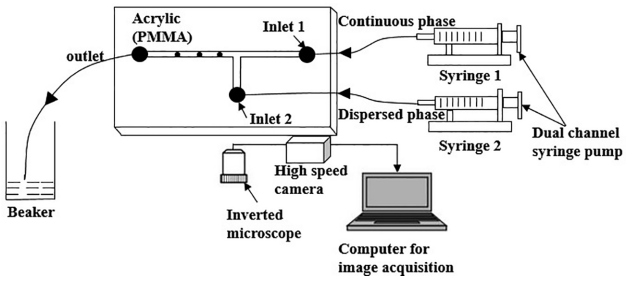

FIG. 2. A schematic of the experimental setup used is shown here. The continuous phase fluid flows from right to left and the dispersed phase in the perpendicular channel with the help of a dual-channel syringe pump. Droplets are formed in the T-junction and move from right to left. The channels are planar having a uniform depth of 200 μm and widths of 300 μm. The cross section of the channel is rectangular.

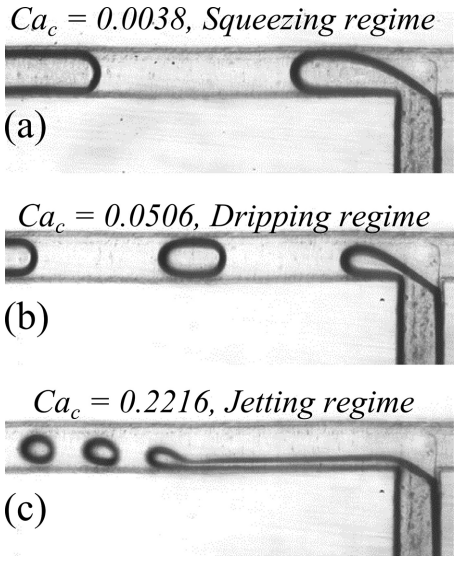

FIG. 3. Experimental images illustrating the water droplet breakup in mineral oil with varying capillary number are shown. The results are shown for the flow rate ratio $\phi = 1$. (a) The droplet breakup occurs in the squeezing regime at a small capillary number, (b) increase in the capillary number causes the droplet breakup in the dripping regime, (c) further increase in the capillary number causes the dispersed phase thread to elongate downstream of the channel and droplet breakup occurs in the jetting regime.

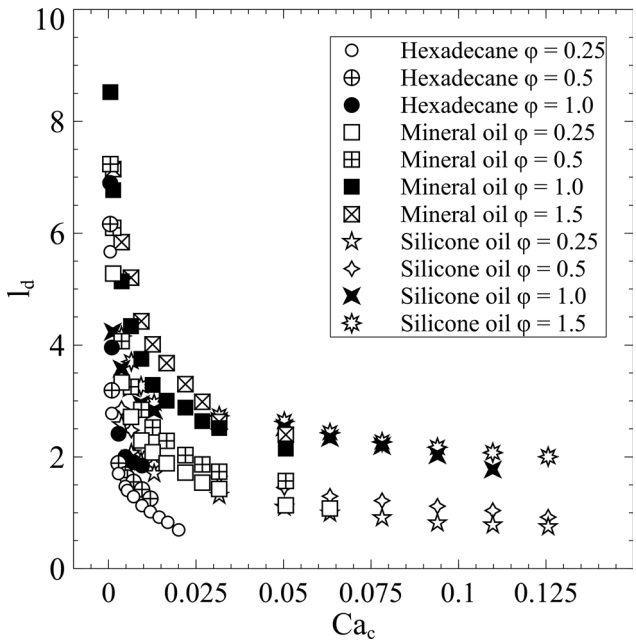

FIG. 4. l_d is plotted against the Ca_c for different λ and ϕ. $\lambda = 0.4167$ for hexadecane ◯, $\lambda = 0.0422$ for mineral oil □, $\lambda = 0.0111$ for silicone oil ★. The non-dimensional length of the droplet l_d decreases with an increasing capillary number Ca_c. The non-dimensional droplet length increases with an increase in the flow rate ratio. However, no particular trend is observed with varying viscosity ratios.

increase in the capillary number of the continuous phase. It was also investigated that there is a sharp transition between regimes at higher λ ($\lambda \sim 10$) for smaller capillary number of continuous phase and droplets were generated in the jetting regime. However, the effect of the viscosity ratio on the non-dimensional length of the droplet does not follow any particular trend. For example, the length of the droplet in the region of low capillary numbers is observed to be larger when mineral oil (with $\lambda = 0.0422$) is used as the continuous phase as compared to hexadecane (with $\lambda = 0.4167$) or silicone oil (with $\lambda = 0.0111$). It is important to reiterate that no existing model can accurately predict the length of the droplet with the varying capillary number.

In order to understand the effect of the dispersed phase Weber number We_d on the droplet breakup, the experimental images of water-in-mineral oil at $Ca_c = 0.0220$ and with varying We_d are shown in Fig. 5. All the images shown in the figure were taken immediately before the kink formation at the interface. At higher We_d, the length of the droplet is observed to be larger. It can also be observed that the thickness of the neck is larger when the dispersed phase Weber number is larger. It leads to the conclusion that the dynamic pressure inside the liquid prevents the formation of kink at the interface until the forces on the continuous phase become sufficiently large. Thus, the

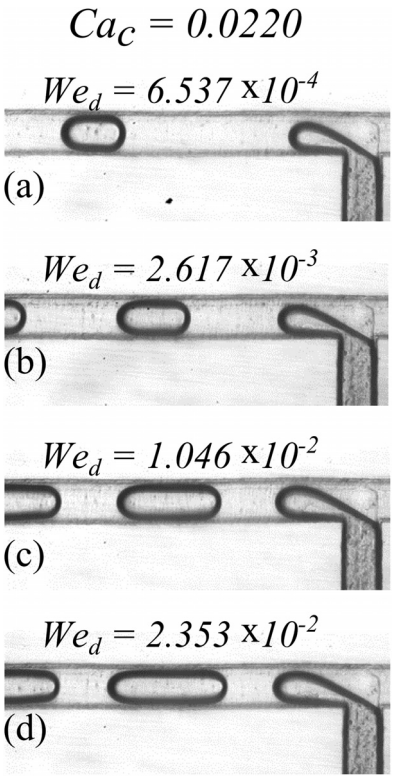

FIG. 5. Experimental images illustrating the water droplet breakup in mineral oil for varying dispersed phase Weber number is shown. The images were taken just before the formation of a kink. The neck length is observed to increase with increasing We_d. It indicates that the increasing dispersed phase inertial forces resist the neck breakup and lead to larger droplet sizes. (a) $We_d = 6.537 \times 10^{-4}$, (b) $We_d = 2.617 \times 10^{-3}$, (c) $We_d = 1.046 \times 10^{-2}$, and (d) $We_d = 2.353 \times 10^{-2}$.

increase in the dispersed phase Weber number delays the droplet breakup and causes the length of the droplet to increase.

Because Eq. (4) suggests that the $l_d Ca_c$ depends solely on $We_d(1+\phi)/2\phi$, the length of the droplets measured from experimental results is plotted in Fig. 6(a), where $l_d Ca_c$ is shown on the vertical axis and $We_d(1+\phi)/2\phi$ is shown on the horizontal axis. From Fig. 6(a), it can be observed that $l_d Ca_c$ collapses onto a single curve for a given continuous phase fluid irrespective of the flow rate ratio, as predicted by Eq. (4). All the data show an increase in $l_d Ca_c$ with an increase in the dispersed phase Weber number until a critical dispersed phase Weber number is reached. The curve thereafter flattens out, and the values of $l_d Ca_c$ become constant. It was observed that the points where the curves flatten indicate the transition from the dripping to jetting regime of droplet breakup. It implies that the jetting regime is independent of the dispersed Weber number. Since the jetting regime of the droplet breakup is a result of instabilities that occur at the interface of an elongated dispersed phase, the droplet length in the jetting regime should depend on the continuous phase capillary number but could be independent of the dispersed phase Weber number. To the authors' knowledge, Eq. (4) is the first relation that shows the effect of dispersed phase inertial forces on droplet generation in T-junction microchannels.

The log–log plot $l_d Ca_c$ vs $We_d(1+\phi)/2\phi$ is shown in Fig. 6(b). The experimental data with varying flow rate ratios are found to collapse into a master curve for vertical and horizontal axes of Fig. 6(b) ranging up to four orders of magnitude, indicating the robustness of the scaling law given by Eq. (4). The plot demonstrates two other noteworthy points. At high $We_d(1+\phi)/2\phi$, the curve shows a plateau. As mentioned earlier, the point of change of slope indicates the transition from the dripping to jetting regime. Second, another plateau is also observed at very low $We_d(1+\phi)/2\phi$. It is important to note that the point where the change of slope occurs at low and high $We_d(1+\phi)/2\phi$ is different for different flow rate ratios and different viscosity ratios. The lower plateau represents the transition to the leaking regime, which occurs at very small flow rates, as suggested by Korczyk *et al.*[36] The data from Korczyk *et al.*[36] is plotted in Fig. S2, and similar characteristics are observed as in Fig. 6(b). In their experiments, Korczyk *et al.* used channels of 360 μm in width and height, and they used hexadecane as the continuous phase and fluorinated oil as the dispersed phase with $\lambda = 1.138$. The results obtained in the present experiments and from Korczyk *et al.*[36] are consistent with the model discussed above.

The results obtained show that the length of the droplet can be estimated using the scaling obtained from Eq. (4), and at varying flow rate collapse into a single curve for a fixed viscosity ratio. However, the curves obtained for different viscosity ratios lie parallel to one another and do not collapse into a universal curve. A universal curve for predicting the droplet sizes can be obtained by determining the relation between $f(w_c/w_g)$ and the viscosity ratios λ and flow rate ratios ϕ. The exact relation cannot be determined in the present study and will necessitate a significant contribution from high fidelity numerical simulations. But to verify the effect of $f(w_c/w_g)$ on the droplet generation, a crude approximation of the function is made in the present study. It was experimentally observed that w_g varies inversely with the viscosity ratio (as shown in Fig. S3) and the relation from the empirical data were approximated as $f(w_c/w_g) \sim \lambda^{0.67}$. By plotting $l_d Ca_c \lambda^{0.67}$ vs $We_d(1+\phi)/2\phi$, as shown in Fig. 6(c), it can be observed that the

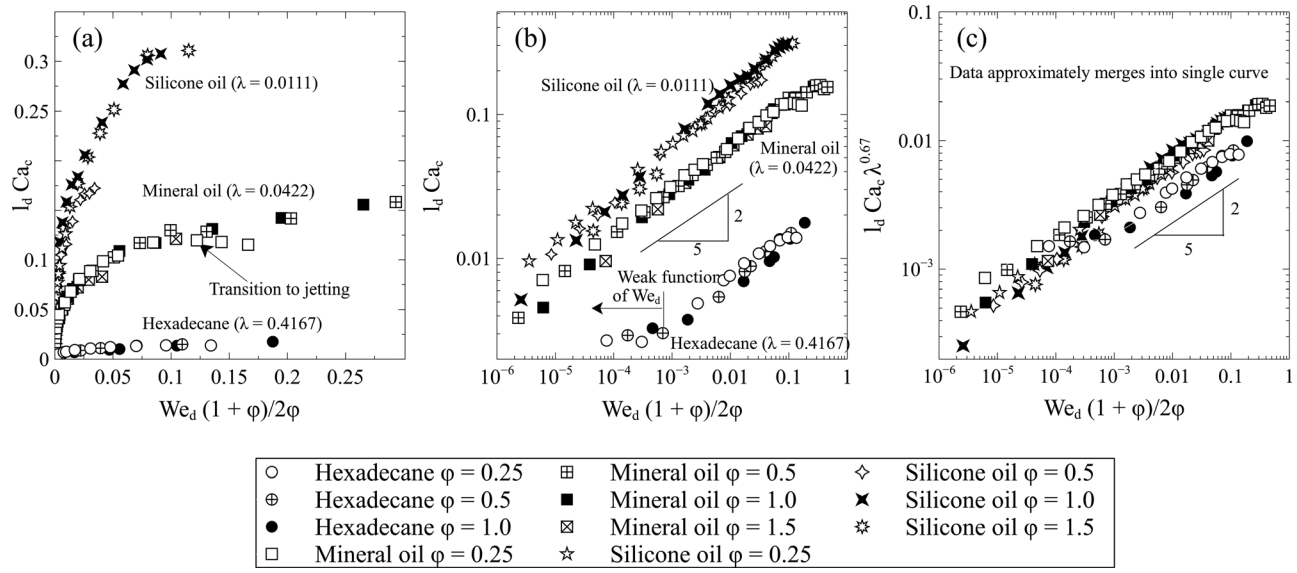

FIG. 6. (a) $l_d Ca_c$ is plotted against the $We_d(1+\phi)/2\phi$ for different λ and ϕ. It can be observed that all the data of one viscosity ratio collapses into one curve irrespective of the ϕ used. Three curves observed in the plot represent three different λ. (b) $l_d Ca_c$ is plotted against the $We_d(1+\phi)/2\phi$ on a log–log scale for different λ and ϕ. It can be observed that the slope of the y-axis with respect to the x-axis is 0.4. Two plateaus appear on the curves, one at high We_d, indicating a transition for dripping to jetting regime and another at low We_d, indicating a weak dependence on We_d. Both higher and lower plateau zones vary with λ and ϕ. (c) $l_d Ca_c \lambda^{0.67}$ is plotted against the $We_d(1+\phi)/2\phi$ on a log–log scale for different λ and ϕ. Here, a crude approximation of $f(w_c/w_g)$ was considered as $\lambda^{0.67}$. It can be seen that the data for varying λ and ϕ almost collapse into one master curve. It suggests that the model developed in the present study can be used to obtain a universal scaling law for predicting the droplet sizes in a T-junction microchannel. However, a detailed analysis on $f(w_c/w_g)$ will be needed.

data for varying viscosity ratios almost collapses into the single master curve. We observe that the data points of hexadecane deviate from the master curve within $O(1)$ magnitudes. Hence, it can be concluded that by determining the exact equations for the function $f(w_c/w_g)$, a universal scaling for droplet length prediction in squeezing and dripping regimes can be obtained.

Earlier studies had shown that an increase in the viscosity of continuous for $\lambda < 1$ will lead to transition for the droplet generation regime to jetting regime where the fluid streams flow parallel to each other. Wehking *et al.*[39] had shown that the transition from plug formation to stable parallel flowing streams increases with an increase in the viscosity ratio. However, within the squeezing regime and the dripping regime, the effect of viscosity ratio on the droplet size has not been discussed in detail. Garstecki *et al.*[23] suggested that the droplet sizes are not affected by the viscosity ratio and are primarily dependent on flow rate ratios. De Menech[40] suggested that the viscosity ratio is relevant in the droplet formation process when both shear stress and pressure differences play a role in droplet breakup. However, there is no simple model predicting the effect of viscosity ratio on droplet sizes.

From Fig. 6(c), it can be observed that for fixed dispersed Weber number and the continuous phase capillary number, the droplet size varies inversely with the viscosity ratio. The change in viscosity ratio at a fixed continuous phase capillary number and the dispersed phase Weber number affects the gap between the interface of the droplet and the main channel wall, w_g, thus affecting the droplet sizes. The earlier studies predicting the effect of viscosity ratio on droplet generation size in T-junction microchannels had indirectly coupled it to the effect of capillary number of the continuous phase. The present model allows the prediction of droplet sizes with viscosity ratio independent of the continuous phase capillary number.

The present study, however, does not account for the effect of surfactants on droplet breakup. It was found that the droplet breakup in the presence of surfactants leads to the same scaling but a different proportionality constant, which could possibly be due to convection of surfactants along the interface during droplet breakup. This was reported by the earlier studies where they had found that the dynamic interfacial tension affects the droplet sizes during the emulsification process.[41,42] We presently lack a detailed theory to rationalize the effects of surfactants, and further studies are necessary to incorporate the effect of surfactant concentration into the present model.

V. CONCLUSIONS

In summary, it is shown that the dispersed phase inertial forces play an important role in determining the size of the droplet in squeezing and dripping regimes along with the continuous phase capillary number. While the earlier studies had tried to predict the size of droplets using the continuous phase capillary number and flow rate ratios between the continuous and dispersed phases, the models could not provide a universal relation. The present model leads to a new scaling law, which can be used to predict the size of the droplets in microfluidic channels irrespective of the flow rate ratios. The large set of experiments conducted in the present study and those from the literature clearly demonstrate the validity of present scaling. While the scaling law used in the present study is not universally applicable as observed from the data obtained from different viscosity ratios, it is shown that by accounting for $f(w_c/w_g)$ in Eq. (4), a universal scaling is possible. The effect of different parameters on the gap between the wall and the

interface of the dispersed phase, which will determine the function $f(w_c/w_g)$, needs a thorough investigation. The present study offers a scaling law behavior, which predicts the droplet sizes during breakup in a T-junction microchannel and an important relation that accounts for the effect of dispersed phase inertial forces on droplet breakup.

However, it should be noted that the model presented in the present study is limited to rectangular cross section channels and for the orthogonal angles of injection. While the cross sections other than rectangular will need the change in force calculations, injection angles of the dispersed phase other than being perpendicular to the main channel have not been verified in the present study. Further experiments to study the applicability of model for varying injection angles of dispersed phase are necessary.

Prediction of the droplet breakup in microchannels is relevant for a wide range of applications of droplet microfluidics such as cell capturing, drug delivery, and emulsion formation.

SUPPLEMENTARY MATERIAL

See the supplementary material for Figs. S1–S3. Figure S1 shows the viscosity curve for mineral oil and silicone oil. Figure S2 shows the validation of the presented scaling law with the existing literature data, and Fig. S3 shows the effect of viscosity ratio on the gap between the interface and the wall of the main channel, w_g.

ACKNOWLEDGMENTS

The authors thank the Robotics Laboratory facility at IIT Bhubaneswar for providing necessary support with the fabrication facility and the Nanostructure and Soft Matter Physics Laboratory for facilitating the viscosity measurements. The authors thank Dr. S. N. Panigrahi for some insightful discussions on the topic. The authors acknowledge the support provided by IIT Bhubaneswar via Grant No. SP076 and by the Department of Science and Technology, Government of India, via Grant No. IMP/2018/000422 for providing support for this research.

DATA AVAILABILITY

The data that support the findings of this study are available from the corresponding author upon reasonable request.

REFERENCES

[1]S.-Y. Teh, R. Lin, L.-H. Hung, and A. P. Lee, "Droplet microfluidics," Lab Chip **8**, 198–220 (2008).
[2]C. N. Baroud, F. Gallaire, and R. Dangla, "Dynamics of microfluidic droplets," Lab Chip **10**, 2032–2045 (2010).
[3]R. Seemann, M. Brinkmann, T. Pfohl, and S. Herminghaus, "Droplet based microfluidics," Rep. Prog. Phys. **75**, 016601 (2012).
[4]L. Shang, Y. Cheng, and Y. Zhao, "Emerging droplet microfluidics," Chem. Rev. **117**, 7964–8040 (2017).
[5]X.-B. Li, F.-C. Li, J.-C. Yang, H. Kinoshita, M. Oishi, and M. Oshima, "Study on the mechanism of droplet formation in T-junction microchannel," Chem. Eng. Sci. **69**, 340–351 (2012).
[6]Y. Zhang, J. Fan, and L. Wang, "Formation of nanoliter droplets in a confined microfluidic T-shaped junction: Formation time and droplet volume," Curr. Nanosci. **5**, 519–526 (2009).
[7]S. Sohrabi, M. K. Moraveji *et al.*, "Droplet microfluidics: Fundamentals and its advanced applications," RSC Adv. **10**, 27560–27574 (2020).
[8]S. Van Loo, S. Stoukatch, M. Kraft, and T. Gilet, "Droplet formation by squeezing in a microfluidic cross-junction," Microfluid. Nanofluid. **20**, 146 (2016).
[9]S. Wu, J. Chen, X. Liu, and F. Yao, "Experimental study of droplet formation in the cross-junction," J. Dispersion Sci. Technol. (published online) (2020).
[10]J. Sivasamy, T.-N. Wong, N.-T. Nguyen, and L. T.-H. Kao, "An investigation on the mechanism of droplet formation in a microfluidic T-junction," Microfluid. Nanofluid. **11**, 1–10 (2011).
[11]P. Kumar and M. Pathak, "Pressure transient during wettability mediated droplet formation in a microfluidic T-junction," Ind. Eng. Chem. Res. **59**, 11839 (2020).
[12]H. Song, D. L. Chen, and R. F. Ismagilov, "Reactions in droplets in microfluidic channels," Angew. Chem., Int. Ed. **45**, 7336–7356 (2006).
[13]J. Chen, D. Chen, Y. Xie, T. Yuan, and X. Chen, "Progress of microfluidics for biology and medicine," Nano-Micro Lett. **5**, 66–80 (2013).
[14]S. Mashaghi, A. Abbaspourrad, D. A. Weitz, and A. M. van Oijen, "Droplet microfluidics: A tool for biology, chemistry and nanotechnology," TrAC Trends Anal. Chem. **82**, 118–125 (2016).
[15]T. S. Kaminski, O. Scheler, and P. Garstecki, "Droplet microfluidics for microbiology: Techniques, applications and challenges," Lab Chip **16**, 2168–2187 (2016).
[16]A. Wang, A. Abdulla, and X. Ding, "Microdroplets-on-chip: A review," Proc. Inst. Mech. Eng., Part H **233**, 683–694 (2019).
[17]Z. Z. Chong, S. H. Tan, A. M. Gañán-Calvo, S. B. Tor, N. H. Loh, and N.-T. Nguyen, "Active droplet generation in microfluidics," Lab Chip **16**, 35–58 (2016).
[18]R. Singh, S. Bahga, and A. Gupta, "Electrohydrodynamic droplet formation in a T-junction microfluidic device," J. Fluid Mech. **905**, A29 (2020).
[19]P. Zhu and L. Wang, "Passive and active droplet generation with microfluidics: A review," Lab Chip **17**, 34–75 (2017).
[20]G. F. Christopher and S. L. Anna, "Microfluidic methods for generating continuous droplet streams," J. Phys. D **40**, R319–R336 (2007).
[21]T. Thorsen, R. W. Roberts, F. H. Arnold, and S. R. Quake, "Dynamic pattern formation in a vesicle-generating microfluidic device," Phys. Rev. Lett. **86**, 4163 (2001).
[22]T. Nisisako, T. Torii, and T. Higuchi, "Droplet formation in a microchannel network," Lab Chip **2**, 24–26 (2002).
[23]P. Garstecki, M. J. Fuerstman, H. A. Stone, and G. M. Whitesides, "Formation of droplets and bubbles in a microfluidic T-junction-scaling and mechanism of break-up," Lab Chip **6**, 437–446 (2006).
[24]M. De Menech, P. Garstecki, F. Jousse, and H. A. Stone, "Transition from squeezing to dripping in a microfluidic T-shaped junction," J. Fluid Mech. **595**, 141–161 (2008).
[25]J. Xu, S. Li, J. Tan, Y. Wang, and G. Luo, "Preparation of highly monodisperse droplet in a T-junction microfluidic device," AIChE J. **52**, 3005–3010 (2006).
[26]G. F. Christopher, N. N. Noharuddin, J. A. Taylor, and S. L. Anna, "Experimental observations of the squeezing-to-dripping transition in T-shaped microfluidic junctions," Phys. Rev. E **78**, 036317 (2008).
[27]Z. Nie, M. Seo, S. Xu, P. C. Lewis, M. Mok, E. Kumacheva, G. M. Whitesides, P. Garstecki, and H. A. Stone, "Emulsification in a microfluidic flow-focusing device: Effect of the viscosities of the liquids," Microfluid. Nanofluid. **5**, 585–594 (2008).
[28]A. Gupta and R. Kumar, "Flow regime transition at high capillary numbers in a microfluidic T-junction: Viscosity contrast and geometry effect," Phys. Fluids **22**, 122001 (2010).
[29]T. Glawdel, C. Elbuken, and C. L. Ren, "Droplet formation in microfluidic T-junction generators operating in the transitional regime. I. Experimental observations," Phys. Rev. E **85**, 016322 (2012).
[30]J. D. Tice, A. D. Lyon, and R. F. Ismagilov, "Effects of viscosity on droplet formation and mixing in microfluidic channels," Anal. Chim. Acta **507**, 73–77 (2004).
[31]H. Liu and Y. Zhang, "Droplet formation in a T-shaped microfluidic junction," J. Appl. Phys. **106**, 034906 (2009).
[32]J. H. Xu, S. Li, J. Tan, and G. Luo, "Correlations of droplet formation in T-junction microfluidic devices: From squeezing to dripping," Microfluid. Nanofluid. **5**, 711–717 (2008).
[33]T. Glawdel, C. Elbuken, and C. L. Ren, "Droplet formation in microfluidic T-junction generators operating in the transitional regime. II. Modeling," Phys. Rev. E **85**, 016323 (2012).
[34]X. Li, L. He, Y. He, H. Gu, and M. Liu, "Numerical study of droplet formation in the ordinary and modified T-junctions," Phys. Fluids **31**, 082101 (2019).

[35]J. Nunes, S. Tsai, J. Wan, and H. A. Stone, "Dripping and jetting in microfluidic multiphase flows applied to particle and fibre synthesis," J. Phys. D **46**, 114002 (2013).
[36]P. M. Korczyk, V. Van Steijn, S. Blonski, D. Zaremba, D. A. Beattie, and P. Garstecki, "Accounting for corner flow unifies the understanding of droplet formation in microfluidic channels," Nat. Commun. **10**, 1–9 (2019).
[37]N.-A. Goy, Z. Denis, M. Lavaud, A. Grolleau, N. Dufour, A. Deblais, and U. Delabre, "Surface tension measurements with a smartphone," Phys. Teach. **55**, 498–499 (2017).
[38]M. Nekouei and S. A. Vanapalli, "Volume-of-fluid simulations in microfluidic T-junction devices: Influence of viscosity ratio on droplet size," Phys. Fluids **29**, 032007 (2017).
[39]J. D. Wehking, M. Gabany, L. Chew, and R. Kumar, "Effects of viscosity, interfacial tension, and flow geometry on droplet formation in a microfluidic T-junction," Microfluid. Nanofluid. **16**, 441–453 (2014).
[40]M. De Menech, "Modeling of droplet breakup in a microfluidic T-shaped junction with a phase-field model," Phys. Rev. E **73**, 031505 (2006).
[41]X. Wang, A. Riaud, K. Wang, and G. Luo, "Pressure drop-based determination of dynamic interfacial tension of droplet generation process in T-junction microchannel," Microfluid. Nanofluid. **18**, 503–512 (2015).
[42]N. M. Kovalchuk, E. Roumpea, E. Nowak, M. Chinaud, P. Angeli, and M. J. Simmons, "Effect of surfactant on emulsification in microchannels," Chem. Eng. Sci. **176**, 139–152 (2018).